

On the Influence of Hot Reducing Gas Injection on Blast Furnace Performance



Authors

Mohammadhossein Alimohammadi (top left), Graduate Research Assistant, Center for Innovation Through Visualization and Simulation (CIVS), Purdue University Northwest, Hammond, Ind., USA
malimoh@pnw.edu

Tyamo Okosun (top right), Research Associate Professor, Center for Innovation Through Visualization and Simulation (CIVS), Purdue University Northwest, Hammond, Ind., USA
tokosun@pnw.edu

Lucas Melton (bottom left), Cleveland-Cliffs Burns Harbor, Burns Harbor, Ind., USA
lucas.melton@clevelandcliffs.com

Cody Hollingshead, Cleveland-Cliffs Burns Harbor, Burns Harbor, Ind., USA
cody.hollingshead@clevelandcliffs.com

Chenn Q. Zhou (bottom right), NIPSCO Distinguished Professor of Engineering Simulation; Founding Director, Center for Innovation Through Visualization and Simulation (CIVS); and Founding Director, Steel Manufacturing Simulation and Visualization Consortium (SMSVC), Purdue University Northwest, Hammond, Ind., USA
czhou@pnw.edu

The steel industry is crucial for the economy but significantly contributes to energy consumption and carbon emissions, impacting global warming. To reduce its carbon footprint and achieve carbon neutrality, nations and manufacturers are developing low-carbon steelmaking technologies. Natural gas injection in blast furnaces can reduce the steelmaking industry's carbon footprint. However, excessive injection can freeze the furnace and lower flame temperatures. This study explores how externally superheated reducing gas, generated by plasma torches or chemical processes such as pyrolysis, can overcome these limitations by providing more sensible heat to the furnace using computational fluid dynamics. The goal is to increase natural gas flow and achieve decarbonization through electrification.

Introduction

The ironmaking and steelmaking industry play a crucial role in modern society. This includes activities that support economic growth, develop infrastructure and provide jobs worldwide. As an important part of this industry, the blast furnace remains an essential technology for turning iron ore into molten steel. The blast furnace (BF) accounts for more than 70% of pig iron production in North America and represents the predominant method for iron production globally. Continuous innovations have improved its efficiency and reduced its emissions, driving the industry toward greater environmental sustainability. Despite these advancements, the steelmaking sector still faces major challenges, particularly high energy consumption and CO₂ emissions. Worldwide, the steel industry contributes approximately 7% of global carbon emissions, with blast furnace ironmaking contributing the majority.^{1,2}

When looking to minimize fuel consumption and CO₂ emissions from blast furnaces, researchers generally aim to reduce reliance on coke. Utilizing new fuel sources within the blast furnace, such as natural gas, synthetic gas (syngas) or waste plastic,

can not only increase the hot metal production rate, but also lowers the consumption of carbon per ton of product, reducing the amount of CO₂ generated.³ Natural gas has emerged as a promising alternative fuel due to its abundance, affordability and the hydrogen it contains, which participates in the reduction reactions, thereby decreasing the furnace's dependence on coke.

Despite the numerous advantages associated with natural gas injection, it also presents certain challenges that must be addressed. When natural gas is injected into the blast furnace, it typically lowers the flame temperature. This reduction in temperature occurs due to natural gas combustion products participating in endothermic reactions with coke, as well as due to natural gas cracking, which absorbs energy, rather than undergoing complete combustion.⁴⁻⁶ To address this, various strategies have been explored. In one study, the influence of lance tip geometry on natural gas injection was examined. The findings indicated that turbulence generated by different lance designs enhanced gas mixing, increasing injection efficiency. However, the elevated temperatures at the tuyere can lead to melting of the lance tip, eventually eroding its

specialized geometry and reverting it to a standard lance shape.⁵ Other studies have investigated preheated natural gas injection in the blast furnace; however, increasing the temperature of natural gas beyond a certain limit led to CH₄ cracking.⁶

Carbon monoxide and hydrogen are the two primary reducing gases used in blast furnaces. These gases play distinct roles in the reduction of iron ore. Hydrogen undergoes endothermic reactions with iron ore, absorbing energy and reducing the hot metal temperature. The byproduct of this process is water. In contrast, carbon monoxide participates in exothermic reactions with iron ore, releasing energy that raises the hot metal temperature, with carbon dioxide as its byproduct. The reduction of iron ore using hydrogen in shaft furnaces is highly endothermic, as the process requires a substantial heat input to drive the chemical reactions. The absence of an internal heat source like coke exacerbates this challenge, lowering the temperature in the bed and impacting the efficiency of reduction. The need for effective heat transfer between the hydrogen and the densely packed iron ore is critical to overcoming this issue, and strategies like optimizing gas flow and improving heat distribution are crucial to enhance performance.^{7,8} Compensating for the energy loss associated with hydrogen's endothermic reactions is one of the key factors limiting the share of H₂ reduction at a target production rate.

Computational fluid dynamics (CFD) has been widely used to assess potential changes in blast furnace operations quickly and cost-effectively. Purdue University Northwest's (PNW's) Center for Innovation Through Visualization and Simulation (CIVS) has developed a comprehensive set of models to simulate the complex physical processes that occur in a blast furnace. These models use a combination of commercial computational fluid dynamics software and specialized modeling code. By combining these tools, researchers can better understand the various aspects of heat transfer, fluid flow, chemical reactions and other important factors that influence blast furnace performance, helping to improve efficiency and reduce environmental impact.^{9–11}

Blast furnace modeling has advanced significantly through the development of computational techniques to optimize performance and understand complex in-furnace phenomena. A three-dimensional (3D) computational fluid dynamics model¹² effectively captures the layered burden, cohesive zone (CZ) behavior, gas and liquid redistribution near raceways, and the impacts of different modeling approaches on coke rate and productivity. To enhance predictions of iron ore reduction and melting processes, a Eulerian-based reduction model¹³ offers a scalable alternative validated against experimental data. Further, the raceway dynamics and combustion have been improved through reactive CFD-discrete element method (CFD-DEM) simulations,¹⁴ significantly reducing computational costs while analyzing raceway morphology, temperature fields and gas species

distributions. The effects of ore and coke sizes on BF operation were explored using a validated 3D multifluid model,¹⁵ revealing critical size thresholds for optimizing thermochemical efficiency. Unified Euler–Lagrange simulation platforms¹⁶ have integrated transient granular and multiphase flows with digital twin technology, achieving efficient and accurate predictions across scales. Additionally, a 3D transient model for co-combustion of pulverized coal and coke¹⁷ elucidates their interactions, showing how blast rate adjustments affect raceway dimensions, coal burnout and reducing gas generation. These works collectively provide valuable insights and tools for enhancing BF performance and stability.

The ironmaking industry continues to explore ways to increase natural gas injection as a fuel in the blast furnace.^{5,6} Natural gas offers a significant advantage because it provides three moles of reducing agents (two moles of hydrogen and one mole of carbon monoxide) for each mole of gas, reducing the reliance on coke as the primary fuel and (particularly in North America) the associated fuel costs for the operation. There are, however, some requirements for balancing gas injection. Increasing natural gas injection typically lowers the flame temperature, which can impact furnace stability to varying degrees. On the other hand, the higher oxygen enrichment levels typically used to raise flame temperatures and maintain energy input result in declining top gas temperatures, potentially leading to operational challenges if temperatures fall below 100°C.¹⁸ Many operations aim to maximize natural gas injection while maintaining the necessary flame temperature for stable operations. One approach to achieve this is by compensating for the flame temperature drop through the addition of sensible heat, which can be supplied using externally heated gas. This method enables higher utilization of natural gas, enhances energy efficiency and reduces reliance on traditional coke. By carefully managing these parameters, blast furnaces can operate efficiently within the desired performance range while minimizing costs and emissions.¹⁹

This work aims to evaluate the impact of superheated reducing gas injection in blast furnaces, particularly on carbon emissions and process efficiency. Externally heated reducing gas injection could serve as a method of providing additional sensible heat melting iron ore in the blast furnace, rather than relying on increased coke combustion via oxygen enrichment. To accomplish this, a baseline case model using 95 kg/THM of natural gas with 28% oxygen enrichment was created based on industry provided information. Two additional cases with added sensible heat via hot reducing gas injection (400 kW and 700 kW of added heat) are compared to this baseline, with both additional scenarios using 95 kg/THM of natural gas and 28% of oxygen enrichment.

Methodology and CFD Models

The blast furnace is a highly complex refractory structure composed of various parts, making it challenging to model the entire system within a single model. One key difficulty arises from the contrasting dynamics within the furnace. For example, in the tuyere region, gas velocities can reach velocities of 200–250 m/second, while the overall burden movement through the furnace takes approximately seven to eight hours. These differences in timescales and velocities make it difficult to create a single comprehensive model. To address this, PNW's blast furnace models use three separate components for the gas-solid reaction regions of differing phenomena: the tuyere, raceway and shaft. The tuyere model was developed using ANSYS Fluent, a commercial CFD software, while the raceway modeling approach uses a combination of commercial and in-house code, and the blast furnace shaft model is an in-house CFD solver. These models work together to predict how the blast furnace may respond to new and different operating conditions.

The first model of the three, the tuyere model, addresses the combustion dynamics, flow patterns and heat transfer occurring in the tuyere due to the hot blast, and coke and injected fuel combustion. It also incorporates the geometric characteristics of the injection design, such as fuel delivery through injection lances and tuyere ports, as well as the properties of the specific fuel used. The tuyere region is simulated using the commercial CFD software ANSYS Fluent, version 2023R1. The finite volume method is utilized for all three model sections to discretize the governing equations such as mass, energy, momentum and continuity are discretized and numerically solved.

As this effort intends to investigate the influence of superheated gas injection, which may enter the tuyere with temperatures near the melting point of steel, it is

important to consider the impacts of radicals upon the gas reactions in the tuyere. To accomplish this, a 28-step reaction mechanism was sourced from literature which includes some of the most important radicals and their influence on the reaction pathways for combustion and decomposition of natural gas and related hydrocarbons. The reaction mechanisms and associated rate constants and activation energies can be seen in Table 2.

By using outlet conditions from the tuyere model as inlet conditions for a secondary model, it is possible to simulate the BF raceway through one-way coupling. This approach integrates a commercial solver to forecast the formation of the raceway with an in-house solver to calculate the reactions of coke and injected fuel. Information on gas mass generation and changes in gas density due to combustion (including temperature and solid-to-gas mass transfer) is exchanged between the two models in an iterative process until a stable raceway shape is reached.^{10,21}

A third in-house model addresses the conditions within the shaft region of the BF. This solver simulates the flow and reactions of the bosh gas entering the shaft from the raceway region, along with coke gasification, ore reduction, and the formation and location of the CZ. The bosh inlet conditions are determined by the raceway model, enabling one-way coupling between the raceway and shaft models, similar to the coupling with the tuyere models. The burden distribution can be calculated based on a charge matrix and rotating chute angles or imported from plant-specific software. Additionally, the solver computes gas–gas and gas–solid heat and mass transfer, flow physics, and chemical reactions, and iteratively determines the CZ region's location. The upper limit of the CZ is set by the ore's softening temperature, while the lower limit is set by its liquidus temperature. These temperatures can be fixed or calculated based on the chemical composition of the charged ore material.

Table 1

Generalized Governing Transport Equations

Mass: $\varphi = 1$
 Momentum: $\varphi = \text{velocity}$
 Energy: $\varphi = \text{enthalpy}$

$$\nabla \cdot (\rho \varphi \mathbf{u}) = \nabla \cdot (\Gamma_{\varphi} \nabla \varphi) - \nabla \cdot (\rho \mathbf{u}' \varphi') + S_{\varphi}$$

Species Transport

$$\nabla \cdot (\rho \mathbf{u} Y_i) = \nabla \cdot (\rho \Gamma_i \nabla Y_i) + R_i + S_i$$

Turbulence Kinetic Energy

$$\nabla \cdot (\rho k \mathbf{U}) = \nabla \cdot \left(\frac{\mu_t}{\sigma_k} \nabla k \right) + 2\mu_t S_{ij} \cdot S_{ij} - \rho \varepsilon$$

Turbulence Dissipation Rate

$$\nabla \cdot (\rho \varepsilon \mathbf{U}) = \nabla \cdot \left(\frac{\mu_t}{\sigma_{\varepsilon}} \nabla \varepsilon \right) + C_{1\varepsilon} \frac{\varepsilon}{k} 2\mu_t S_{ij} \cdot S_{ij} - C_{2\varepsilon} \rho \frac{\varepsilon^2}{k}$$

where

$$\mu_t = C_{\mu} \rho \nu l = \rho C_{\mu} \frac{k^2}{\varepsilon}$$

The CZ shape is updated every 300 simulation iterations based on predicted changes in burden temperatures.^{9,11,15}

Geometry

The blast furnace modeled is a typical North American furnace located at Cleveland-Cliffs Burns Harbor, with 28 tuyeres, a hearth diameter of ~10 m and working volume of ~2,600 m³. A standard tuyere at this furnace utilizes a twin-lance design originally injected for natural gas and coal injection. Current operations utilize only gas injection, with the flow divided evenly between both lances. In this study, a new injection lance geometry is proposed for delivery of the superheated reducing gas using a co-annular lance wherein hot reducing gas is transported through a central lance, while the additional natural gas flow through the annular lance serves to cool the system. The standard design and co-annular lance design can be compared in Fig. 1. It is noted that the additional turbulence generated via mixing of gas streams may also enhance the combustion rate of natural gas and improve burnout.

The injection of superheated reducing gas (expected at up to 2,000 K) raises some operational concerns. Firstly, the high temperature of the gas could result in lance damage if deployed in the standard dual-lance design. The co-annular lance design aides in preventing this, but results in the potential for overheating of injected natural gas under certain conditions, which might lead to coking and blockages in the annular lance. Second, such high-temperature gas could result in refractory or tuyere damage if impinging on the inner wall of the tuyere or blowpipe. Finally, the reduced

Table 2

Reaction Mechanisms, Activation Energies and Rate Constants Used in the Tuyere Region²⁰

	Reactions	$k = AT^b \exp(E_a/RT)$		
		A (mol cm s K)	b	E _a (cal/mol)
1	OH + H ₂ = H ₂ O + H	2.14E + 08	1.52	3,449
2	H + O ₂ = OH + O	1.00E + 14	0	14,850
3	H + O ₂ + M = HO ₂ + M; γ _{H₂O} = 12, γ _{H₂} = 1.82, γ _{O₂} = 0.6	2.60E + 15	0	-1,350
4	OH + HO ₂ = H ₂ O + O ₂	2.89E + 13	0	-497
5	H + HO ₂ = H ₂ + O ₂	4.28E + 13	0	1,411
6	O + HO ₂ = O ₂ + OH	3.25E + 13	0	0
7	OH + OH = O + H ₂ O	4.33E + 03	2.70	-2,485
8	O + O + M = O ₂ + M	1.89E + 13	0	-1,788
9	HO ₂ + HO ₂ = H ₂ O ₂ + O ₂	4.20E + 14	0	12,000
10	H ₂ O ₂ + M = OH + OH + M	1.21E + 17	0	45,507
11	CH ₄ + O ₂ = CH ₃ + HO ₂	3.97E + 13	0	56,900
12	CH ₄ + O = CH ₃ + OH	6.90E + 08	1.56	8,485
13	CH ₄ + OH = CH ₃ + H ₂ O	1.60E + 06	2.10	2,460
14	CH ₄ + H = CH ₃ + H ₂	1.33E + 04	3.00	8,034
15	CH ₄ + HO ₂ = CH ₃ + H ₂ O ₂	9.04E + 12	0	24,640
16	CH ₃ + O ₂ = CH ₃ O + O	1.32E + 14	0	31,400
17	CH ₃ + O ₂ = CH ₂ O + OH	3.31E + 11	0	8,942
18	CH ₃ + H = CH ₄	2.11E + 14	0	0
19	CH ₃ + HO ₂ = CH ₃ O + OH	1.81E + 13	0	0
20	CH ₃ O + M = CH ₂ O + H + M	4.30E + 17	0	27,820
21	CH ₂ O + O ₂ = HO ₂ + HCO	6.03E + 13	0	40,685
22	CH ₂ O + O = HCO + OH	3.60E + 13	0	3,460
23	CH ₂ O + OH = HCO + H ₂ O	3.43E + 09	1.18	-447
24	CH ₂ O + H = HCO + H ₂	2.28E + 10	1.05	3,279
25	HCO + O ₂ = HO ₂ + CO	3.31E + 12	0	0
26	CO + O ₂ = CO ₂ + O	1.26E + 13	0	47,060
27	CO + OH = CO ₂ + H	1.51E + 07	1.30	-758
28	CO + HO ₂ = CO ₂ + OH	5.80E + 13	0	22,934

Table 3

Reactions Included in the Base Computational Fluid Dynamics (CFD) Shaft Model²²

Reaction	Chemical Equation
Reduction of iron ore by CO	$3\text{Fe}_2\text{O}_3(\text{s}) + \text{CO}(\text{g}) \rightarrow 2\text{Fe}_3\text{O}_4 + \text{CO}_2(\text{g})$
	$\text{Fe}_3\text{O}_4 + \text{CO}(\text{g}) \rightarrow 3\text{FeO}(\text{s}) + \text{CO}_2(\text{g})$
	$\text{FeO}(\text{s}) + \text{CO}(\text{g}) \rightarrow \text{Fe}(\text{s}) + \text{CO}_2(\text{g})$
Reduction of iron ore by H ₂	$3\text{Fe}_2\text{O}_3(\text{s}) + \text{H}_2(\text{g}) \rightarrow 2\text{Fe}_3\text{O}_4 + \text{H}_2\text{O}(\text{g})$
	$\text{Fe}_3\text{O}_4 + \text{H}_2(\text{g}) \rightarrow 3\text{FeO}(\text{s}) + \text{H}_2\text{O}(\text{g})$
	$\text{FeO}(\text{s}) + \text{H}_2(\text{g}) \rightarrow \text{Fe}(\text{s}) + \text{H}_2\text{O}(\text{g})$
Boudouard reaction	$\text{C}(\text{s}) + \text{CO}_2(\text{g}) \rightarrow 2\text{CO}(\text{g})$
Water gas reaction	$\text{C}(\text{s}) + \text{H}_2\text{O}(\text{g}) \rightarrow \text{CO}(\text{g}) + \text{H}_2(\text{g})$
Flux decomposition	$\text{MeCO}_3(\text{s}) \rightarrow \text{MeO}(\text{s}) + \text{CO}_2(\text{g})$ (Me = Ca, Mg)
Water gas shift reaction	$\text{H}_2(\text{g}) + \text{CO}_2(\text{g}) \rightarrow \text{H}_2\text{O}(\text{g}) + \text{CO}(\text{g})$
Direct reduction of liquid FeO	$\text{C}(\text{s}) + \text{FeO}(\text{l}) \rightarrow \text{Fe}(\text{l}) + \text{CO}(\text{g})$

density of the superheated reducing gas might also result in velocities high enough to choke flow within the injection lance either for the dual lance or the co-annular lance geometries. Each of these concerns are discussed and addressed in the next section.

The methodology for calculating the outer lance diameter in this proposed geometry is that the velocity of natural gas and superheated gas are considered to be the same ($V_{\text{NG}} = V_{\text{SHG}}$). Using this methodology, a diameter ratio can be determined.

Results and Discussion

The results presented in this study are based on a calibrated baseline model informed by industry-provided operating conditions. The baseline operating conditions used for model calibration included an injection rate of 95 kg of natural gas per ton of hot metal (THM), blast at 28% oxygen enrichment, and a target production rate of ~6,600 metric tons of hot metal per day, with a coke rate of ~360 kg/THM, was utilized for model calibration. The validated baseline simulation aligned well with industry data, yielding a difference in predicted production rate of 1.2% (6,517 metric tons/day) and a coke rate prediction within 0.5% of industrial values. Extrapolating from these baseline conditions, this study categorizes results for superheated reducing gas injection into three sections — tuyere, raceway and shaft — reflecting the comprehensive modeling approach employed to simulate the blast furnace's complex processes.

The comparison scenarios selected for this study utilized identical operating conditions to the baseline save for the delivery of superheated H₂ gas through the central pipe of the co-annular lance at 2,000 K and a rate of 6.7 kg/THM, achieving 400 kW of external heating per tuyere, and at a rate of 11.7 kg/THM, achieving 700 kW of external heating per tuyere. The cases were defined thusly to avoid lance overheating by maintaining a consistent gas injection temperature, varying sensible heat input by directly delivering more hot reducing gas (HRG) at the chosen temperature of 2,000 K. Fig. 2 details the differences in gas temperature distributions

Figure 1

Dual-lance geometry of BHC (a), proposed co-annular superheated gas injection lance (b) and an isometric view of the co-annular lance (c).

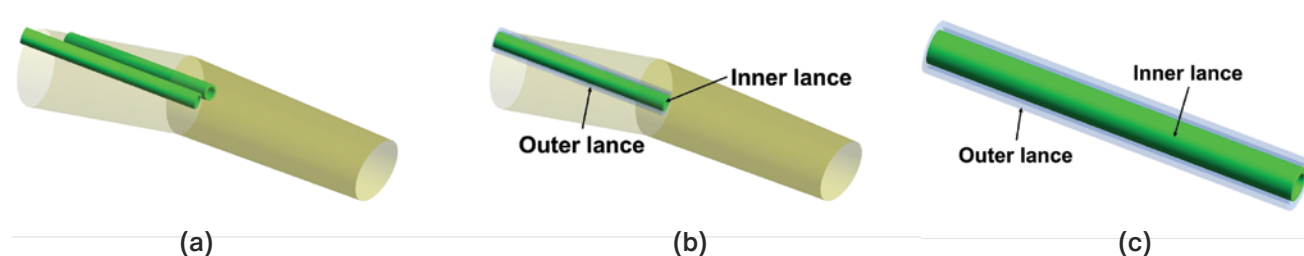


Table 4

Lance Geometry Specification

Geometry specifications	Inner lance	Outer lance
Inside diameter (inch)	1	1.7
Thickness (inch)	0.15	0.15

between the baseline and the superheated gas injection scenario. When injecting natural gas alone, a cold core of gas persists to the outlet of the tuyere. In comparison, when injecting the superheated reducing gas, injected fuel temperatures are generally closer to the blast temperature, resulting in a larger combustion region.

As shown in Table 5, the addition of superheated reducing gas results in increased fluid velocities within the tuyere. The tuyere outlet velocity rises by roughly 10%. To prevent choked flow within the inner lance, the Mach number was calculated for varying operating conditions for the given gas temperature of 2,000 K. To avoid

sonic regimes and the need for compressible flow simulation techniques, the Mach number should be held below 0.6, informing the maximum flowrates of gas through the inner lance for this design. Under these limitations, the maximum flowrate for injected HRG is roughly 19 kg/THM of H_2 , carrying a sensible heat rate of 1.1 MW per tuyere.

Conditions within the raceway region reveal more variations between the two cases, and operational impacts can be observed, as shown in Table 6. In particular, it is noted that despite the reduced O_2 enrichment in the hot blast, total natural gas burnout is increased when injected superheated H_2 gas through the co-annular lance arrangement. This is likely due to the enhanced mixing of natural gas and oxygen generated by geometry modifications. The raceway flame temperature declines by roughly $50^\circ C$ with the addition of the superheated gas, due to the increased gas injection and decreased O_2 enrichment.

As shown in Fig. 3, in both scenarios, the region with the highest hydrogen concentration also exhibits the lowest temperature. This behavior is primarily due to the endothermic reactions of natural gas (cracking) and H_2O from natural gas and H_2 combustion, which reacts with coke in endothermic reactions. This results in similar

Figure 2

Temperature distributions in the tuyere region for the baseline (a) and 6.7 kg/THM superheated reducing gas injection (b).

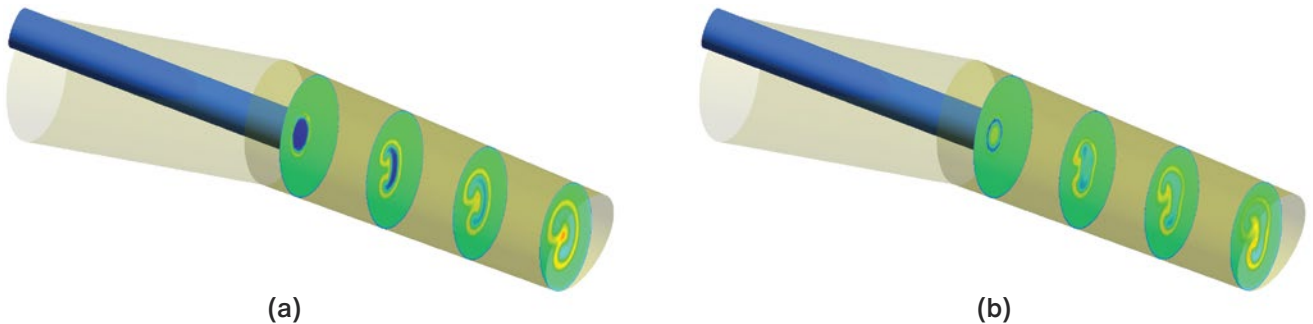


Table 5

Tuyere Region Simulation Results

	O_2 enrichment %	SHG MFR (kg/THM)	CH_4 MFR (kg/thm)	Outlet temperature ($^\circ C$)	Outlet velocity (m/second)
Baseline	28	0	95	1,216	244
400 kW	28	6.70	95	1,246	262
700 kW	28	11.70	95	1,267	275

temperature profiles across the raceway region, although H_2 content in the bosh gas rises significantly with the additional H_2 injection, as expected.

At the highest level, the shaft region results indicate the benefits of the adjusted operating conditions investigated in this study. Table 7 details the differences observed in hot metal temperature, production and coke rate for each scenario. With the adjusted oxygen enrichment and natural gas injection rate, the hot metal temperature ($1,477^\circ\text{C}$), production rate (6,676 THM/day), and top gas temperature (174°C) remained mostly consistent between the baseline and the 700 kW case. Even in the 400 kW case, the higher hot metal temperature provides sufficient headroom to reduce oxygen enrichment, potentially achieving a lower coke rate than stated by these results. As shown in Table 7, modeling predicts that the blast furnace could maintain normal operating conditions with hot reducing gas injection, with stable top gas and hot metal temperatures, and reasonable gas utilization rates.

It should be noted that the cohesive zone height (Fig. 4) is also maintained at the stable baseline level, despite the decreased raceway flame temperatures observed in the superheated reducing gas scenario. However, the operational adjustments enabled using this low flowrate of superheated gas achieved 10 kg/THM in coke rate reduction for the 400 kW case and 17 kg/THM for the 700 kW case. These reductions highlight the successful substitution of coke with injected hot reducing gas, maintaining operating conditions at a target level while reducing coke consumption and carbon emissions. Despite the reduced flame temperatures observed in modeling of the 400 kW and 700 kW HRG scenarios, hot metal temperatures and cohesive zone heights are stable. Implicit to these results is then the additional headroom enabled by hot reducing gas injection. Slight reductions in oxygen enrichment or wind rate with other conditions held fixed could potentially achieve even lower coke rates for the target productivity observed in the baseline (6,600 tons per day), while increased wind rates or oxygen enrichment in combination with higher levels of gas injection might allow for operation beyond what might once have appeared to be stability limits. Finally, it is noted that the use of a hot CO/H_2 blend rather than

Table 6

Raceway Region Simulation Results

	CH_4 MFR (kg/thm)	O_2 enrichment %	Flame temperature ($^\circ\text{C}$)	Overall CH_4 burnout %
Baseline	95	28%	2,038	59.3%
400 kW	95	28%	1,912	43.5%
700 kW	95	28%	1,905	43.7%

H_2 alone would likely avoid or mitigate the declining hot metal temperatures observed with increasing HRG rates (seen here when increasing from “400 kW” to “700 kW”), further widening the window for coke replacement.

Carbon dioxide emission reduction is a primary objective in nearly all hydrogen-related research, including this study. To assess CO_2 emission reduction in a blast furnace equipped with hot reducing gas injection, it is first necessary to identify the sources of CO_2 emissions within the furnace. Nearly all carbon introduced into the blast furnace is converted to CO_2 , with only a negligible fraction retained in molten steel. The primary carbon sources in the blast furnace are the injected natural gas and coke, the latter containing 89.7% carbon. The carbon rate in the blast furnace can be determined using the following equation:

Figure 3

Distributions of gas temperature (top) and H_2 mass fraction (bottom) in the raceway region for the baseline (first column) and 400 kW sensible heat (second column) and 700 kW sensible heat (third column) scenarios.

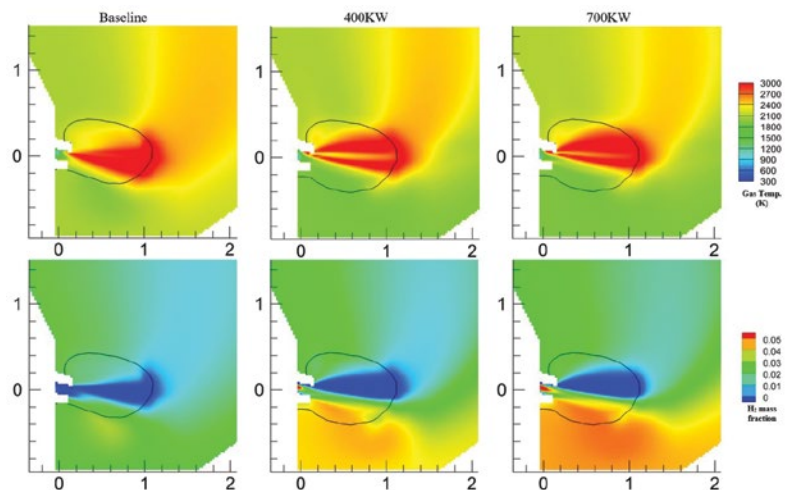


Table 7

Shaft Model Simulation Results

	Baseline operation	400 kW	700 kW
O ₂ enrichment (%)	28	28	28
Superheated H ₂ rate (kg/THM)	0	6.7	11.7
Hot metal temperature (°C)	1,461	1,514	1,477
Coke rate (kg/THM)	361	351	344
H ₂ utilization %	45.6	44.5	44.0
CO utilization %	49.2	50.2	50.7
Production rate (metric THM/day)	6,517	6,554	6,676
Top gas temperature (°C)	155.9	165.9	174.0

$$\begin{aligned} \text{Carbon Rate [kg / THM]} = & \\ & (\text{Real Natural Gas Rate [kg / THM]} \times 0.75) + \\ & (\text{Coke Rate [kg / THM]} \times 0.897) \end{aligned} \quad (\text{Eq. 1})$$

Figure 4

Temperature contour in the shaft region.

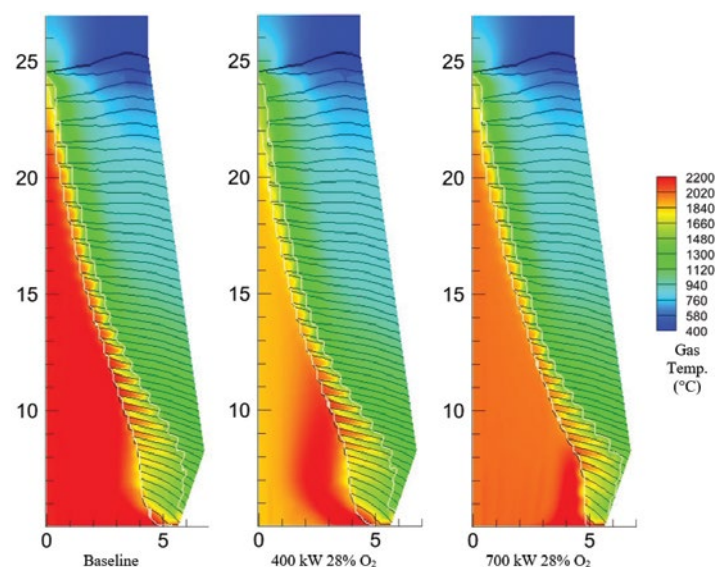


Table 8

Calculated CO₂ Emissions Reductions Based on Modeled Scenarios

	Carbon rate (kg/THM)	Carbon reduction (kg/THM)	CO ₂ reduction (kg/THM)
Baseline	392.5	0	—
400 kW	386.5	6	22.0
700 kW	381.0	11.5	42.4

Assuming that nearly all carbon used in the furnace is converted to CO₂ through reduction reactions or combustion of offgases from the furnace and steelmaking, the CO₂ rate can be estimated using the ratio of carbon to CO₂ molecular weights. Table 8 provides a summary of the emissions reductions associated with the modeling scenarios presented in this article.

Modeling results indicate that hot reducing gas injection, even at low rates, can directly impact CO₂ emissions with very minor changes to blast furnace operating conditions. For the 400 kW injection scenario, CO₂ emissions decrease by 1.5%, while at increased 700 kW injection (with a higher rate of hot H₂), a 2.9% reduction is achieved. At a production rate of roughly 6,600 metric tons per day, this would reduce CO₂ emissions by ~100,000 metric tons per year without any additional adjustments. Modifications to wind rate or oxygen enrichment could potentially enable higher rates of reducing gas or natural gas injection, further reducing emissions.

Conclusion

This study has investigated the potential of heated reducing gas injection to broaden the operating window for blast furnaces and reduce carbon emissions. This innovative approach addresses the challenges associated with high rates of natural gas injection, including reduced flame temperatures and incomplete combustion, by providing an additional source of sensible heat to the furnace, which may have previously been limited by stove capacity. The findings from this study highlight several advantages, such as reductions in coke consumption, decreased emissions, and the enabling of higher gas

injection rates. Additional research to determine the upper limits of injection enabled by external gas superheating could reveal new boundaries around the common expectations for lowest possible coke rates required for stable operation at standard productivity.

Acknowledgments

The authors acknowledge the Steel Manufacturing Simulation and Visualization Consortium ironmaking project technical committee and personnel at Cleveland-Cliffs Inc. for supporting this research work by providing

feedback and collaborative guidance during the development of the simulations. Support from staff and students at the Center for Innovation Through Visualization and Simulation are also greatly appreciated. This research was supported in part by the U.S. Department of Energy's Office of Energy Efficiency and Renewable Energy under the Industrial Efficiency and Decarbonization Office Award Number DE-EE0009390. The views expressed herein do not necessarily represent the views of the U.S. Department of Energy or the United States Government.

This article is available online at AIST.org for 30 days following publication.

References

1. World Steel Association, "Steel Statistical Yearbook 2020, concise version," <https://worldsteel.org/wp-content/uploads/Steel-Statistical-Yearbook-2020-concise-version.pdf> Accessed 9 July 2024.
2. "Iron and Steel Technology Roadmap," International Energy Agency, IEA Publications, Paris, France, 2020.
3. S. Yelluripati, "CFD Analysis of Novel Alternative Injected Fuels in Blast Furnaces," thesis, Purdue University Graduate School, 2024, <https://doi.org/10.25394/PGS.28020968.v1>.
4. K. Wang, H. Zhou, Y. Si, S. Li, P. Ji, J. Wu, J. Zhang, S. Wu and M. Kou, "Numerical Analysis of Natural Gas Injection in Shougang Jingtang Blast Furnace," *Metals*, Vol. 12, No. 12, 2022, p. 2107, <https://doi.org/10.3390/met12122107>.
5. A.K. Silaen, T. Okosun, Y. Chen, B. Wu, J. Zhao, Y. Zhao, J. D'Alessio, J. Capo and C.Q. Zhou, "Investigation of High-Rate Natural Gas Injection Through Various Lance Designs in a Blast Furnace," *AISTech 2015 Conference Proceedings*, 2015, pp. 1536–1549.
6. T. Okosun, S. Nielson, J. D'Alessio, M. Klaas, S.J. Street and C.Q. Zhou, "Investigation of High-Rate and Preheated Natural Gas Injection in the Blast Furnace," *AISTech 2019 Conference Proceedings*, 2019.
7. M.N.A. Tahari, F. Salleh, T.S.T. Saharuddin, A. Samsuri, S. Samidin and M.A. Yarmo, "Influence of Hydrogen and Carbon Monoxide on Reduction Behavior of Iron Oxide at High Temperature: Effect on Reduction Gas Concentrations," *International Journal of Hydrogen Energy*, Vol. 46, No. 48, 2021, pp. 24791–24805.
8. Y. Feu, X. Guan, S. Kuan, A. Yu and N. Yang, "A Review on the Modeling and Simulation of Shaft Furnace Hydrogen Metallurgy: A Chemical Engineering Perspective," *ACS Engineering*, Vol. 4, No. 2, 2023, pp. 145–165.
9. D. Fu, "Numerical Simulation of Ironmaking Blast Furnace Shaft," Ph.D. dissertation, Purdue University, 2014.
10. T. Okosun, "Numerical Simulation of Combustion in the Ironmaking Blast Furnace Raceway," Ph.D. dissertation, Purdue University, 2018.
11. T. Okosun, A. Silaen and C. Zhou, "Review on Computational Modeling and Visualization of the Ironmaking Blast Furnace at Purdue University Northwest," *Steel Research International*, Vol. 90, 2019, p. 16.
12. L. Jiao, S. Kuang, A. Yu, Y. Li, X. Mao and H. Xu, "Three-Dimensional Modeling of an Ironmaking Blast Furnace With a Layered Cohesive Zone," *Metallurgical and Materials Transactions B*, Vol. 51, 2020, pp. 258–275.
13. M. Bösenhofer, F. Hauenberger, H. Stocker, C. Feilmayr and M. Harasek, "An Eulerian-Based Reduction Model for Iron Ore Particle Reduction," *AISTech 2023 Conference Proceedings*, 2023, pp. 358–365.
14. D. Xu, S. Wang and Y. Shen, "An Improved CFD-DEM Modelling of Raceway Dynamics and Coke Combustion in an Industrial-Scale Blast Furnace," *Chemical Engineering Journal*, Vol. 455, 2023, 140677.
15. L. Jiao, X. Zhang, S. Kuang, A. Yu, "Numerical Investigation of Particle Size on the Performance of Ironmaking Blast Furnace," *Metallurgical and Materials Transactions B*, Vol. 55, No. 5, 2024, pp. 3387–3406.
16. B. Peters, "The First Unified and Transient Modeling Platform to Build a Digital Twin of Blast Furnaces Based on the Extended Discrete Element Method," *Steel Research International*, Vol. 95, No. 3, 2024, 2300382.
17. Y. Zhuo and Y. Shen, "Three-Dimensional Transient Modelling of Coal and Coke Co-Combustion in the Dynamic Raceway of Ironmaking Blast Furnaces," *Applied Energy*, Vol. 261, 2020, 114456.
18. N. Patel, M. Sukhram, I. Cameron, V. Subramanyam, A. Gorodetsky and M. Huerta, "The Use of Plasma Torches in Blast Furnace Ironmaking," *Journal of Cleaner Production*, Vol. 495, 2025, 144896.
19. M. Geerdes, R. Chigneau, I. Kurunov, O. Lingardi and J. Ricketts, *Modern Blast Furnace Ironmaking: An Introduction*, IOS Press, Amsterdam, The Netherlands, 2015, pp. 70–75.
20. M. Jazbec, D.F. Fletcher and B.S. Haynes, "Simulation of the Ignition of Lean Methane Mixtures Using CFD Modelling and a Reduced Chemistry Mechanism," *Applied Mathematical Modelling*, Vol. 24, No. 8-9, 2000, pp. 689–696.
21. O.J. Ugarte, T. Okosun, S. Nielson and C.Q. Zhou, "Correlating Impacts of Injected Fuels on Carbon Emissions in Blast Furnace with Computational Fluid Dynamics Modeling," *Steel Research International*, Vol. 94, No. 12, 2023, 2300188.
22. S. Nielson, T. Okosun, O. Ugarte and C.Q. Zhou, "Investigating the Use of Shaft-Level Tuyere Injection With Computational Fluid Dynamics," *AISTech 2023 Conference Proceedings*, 2023, DOI: 10.33313/387/040. ◆